International Journal of Engineering

Journal Homepage: www.ije.ir

Analytical Solution of Electromagnetic Force on Nanofluid Flow with Brownian Motion Effects Between Parallel Disks

E. Tayari[a], L. Torkzadeh*[a], D. Domiri Ganji[b], K. Nouri[a]

[a] Department of Mathematics, Faculty of Mathematics, Statistics and Computer Sciences, Semnan University, Semnan, Iran
[b] Department of Mechanical Engineering, Babol Noushirvani University of Technology, Babol, Iran

P A P E R I N F O	*A B S T R A C T*
	The innovation of the present paper is the analytical study of Brownian motion effects on nanofluid flow and electromagnetic force between parallel disks with a heat source. Nanoparticle effects on nondimensional temperature field and velocity of fluid flow were analyzed using Akbari-Ganji's Method and radial basis function approximation based on Hardy multiquadric function. Akbari-Ganji's Method (AGM) is a strong analytical method that solves any linear and nonlinear differential equation with any degree of variables. Radial basis functions is an approximation method for analyzing functions and equations at high degrees, especially when it is necessary to apply the interpolation problem for scattered data on irregular geometry. The results signified that the maximum difference between AGM and RBF methods, for nondimensional horizontal velocity on CuO nanofluid at $Sq = 1$ and $\eta = 0$ is 0.2251 and the minimum difference for the nondimensional vertical velocity of Al_2O_3 nanofluid at $\eta = 0$ is equal to 0.0018. Also, the effects of the Hartmann number (Ha) on nondimensional horizontal and vertical velocities field for Al_2O_3 nanoparticles at $\eta = 0$ have a slight difference from the other Hartmann values using the AGM method. The maximum of nondimensional horizontal velocities at $\eta = 0$ and $Ha = 8$ is equal to 1.9354.

NOMENCLATURE

a	Compressed parameter	μ_f	viscosity of fluid (kg/m.s)
k	thermal conductivity (W/m. K)	μ_{static}	effective viscosity of the component static (kg/m.s)
B	magnetic field	$\mu_{Brownian}$	effective viscosity of Brownian motion part (kg/m.s)
B_0	primary magnetic field	μ_{eff}	effective viscosity (kg/m.s)
S	heat source	F	electromagnetic force (N)
S_0	primary heat source	Pr_f	electromagnetic force (N)
H	place of the plate (m)	Sq	squeeze number $\left(a\frac{H^2}{2v_f}\right)$
u, v	vlosity components	Ha	hartmann number $\left(H.B_0.\sqrt{\frac{\sigma_f}{\mu_f}}\right)$
x, y	coordinates (m)	ϕ	nanofluid volume fraction
r_j	euclidean norm	d_s	particle diameter (m)
x_j	centers of radial base function	ρ_{nf}	density of nanofluid (kg/m3)
Ψ	polynomial	ρ_f	density of fluid (kg/m3)
N	number of the distinct points at RBF	ρ_s	density of nanoparticles (kg/m3)
λ_j	interpolation coefficient at RBF	σ_{nf}	electrical conductivity of nanofluid (s/m)
ϵ	shape parameter	σ_f	electrical conductivity of fluid (s/m)
T	temperature (K)	σ_s	electrical conductivity of nanoparticles (s/m)

*Corresponding Author Institutional Email: torkzadeh@semnan.ac.ir (L. Torkzadeh)

θ	nondimensional temperature	k_{nf}	thermal conductivity of nanofluid (W/m.K)
$\vec{J}$	electric current	k_f	thermal conductivity of fluid (W/m.K)
k_s	thermal conductivity of nanoparticles (W/m. K)	**Subscripts**	
k_{static}	effective thermal conductivity of the component static (W/m. K)	nf	nanofluid
$k_{Brownian}$	effective thermal conductivity of Brownian motion part (W/m. K)	s	solid
k_{eff}	effective thermal conductivity (W/m.K)	f	fluid
μ_{nf}	viscosity of nanofluid (kg/m.s)	eff	effective

1. INTRODUCTION

Electromagnetic effects on a nanofluid with squeezing flow and Brownian motion effects between two parallel disks have been analytically investigated. Squeezing flow is used in industrial applications such as metallurgy, magnetic hydrodynamic (MHD) generators [1], and petroleum industries. Asefi et al. [2] examined the hydromagnetic flow of a micropolar fluid on a tensile sheet with unstable properties. Also, they investigated the conduction heat transfer numerically with ununiformed heat sources. Ravindran et al. [3] studied the effects of chemical reaction, heat generation, and absorption on unstable MHD flow. This process takes place on top of a vertical cone with ununiformed mass transfer. Motahar [4] studied the effect of entropy production on the magnetic hydrodynamic magnetic flow of a nanofluid in a vertical channel. Asgari and Tariverdilo [5] studied the flow of the MHD boundary layer of an Oldroyd-B fluid in the vicinity of the vertical stretching sheet. They used a non-thermal flux to define the equilibrium energy relation. Han et al. [6,7] studied the significance of Hall current and Joule heating on the dynamics of Darcy–Forchheimer peristaltic flow of Rabinowitsch fluid and also studied partial slips and temperature Jumps of a nanofluid flow over a stretched or shrinking surface. Rashidi et al. [8] studied the modeling and analysis of sensitivity and thermal conductivity of water-based ethylene glycol nanofluids with alumina nanoparticles. Alagumalai et al [9] studied conceptual analysis framework development to understand barriers to nanofluid commercialization. Nouri et al. [10, 11] and Dadsetadi et al. [12] analytically and numerically investigated the system of fractional differential equations based on the hybrid functions. Pourziaei Araban et al. [13] numerically surveyed a cavity with heat source using the lattice Boltzmann method based on the D3Q19 model and compared with experimental results.

In the present study, a combination of squeezing flow with Brownian motion effects and electromagnetic force is modeled to improve the thermal field between two parallel disks with a heat source. All numerical implementations and executions have been done by Maple software to investigate the nondimensional temperature and velocity field due to nanoparticle effects and a heat source between two parallel disks with electromagnetic boundary conditions, alongside hardware configuration: Core (TM) i3-7130U CPU @ 2.70 GHz 2.71 GHz 4GB RAM. First, with the similarity transformation, the governing equations with partial differential equations (PDE) transform to a set of nonlinear ordinary differential equations (ODE). These equations are simulated according to their boundary conditions with AGM and RBF based on Hardy multiquadric (MQ) function. Finally, to study more precisely, the Hartmann number, the squeeze number, and the heat source parameter between two parallel disks have been investigated.

2. PROBLEM DEFINITION

According to Figure 1, if we consider the bottom disk at $z = 0$, the upper disk is located at $z = 2H\sqrt{(1 - at)}$. H is a place of the plate at $z = 0$. a is a compressed parameter that at $a > 0$, referred two plates were compressed until $t = 1/a$ and so, at $a < 0$, two plates separated from each other. In this case, the general governing equations on physics of the problem are as follows:

$$\vec{\nabla}.\vec{V} = 0 \tag{1}$$

$$\rho \frac{\partial \vec{V}}{\partial t} = -\vec{\nabla}\vec{p} + \mu\nabla^2\vec{V} + \vec{F} \tag{2}$$

$$\frac{\partial T}{\partial t} = \frac{k}{\rho C_p}\nabla^2 T + \frac{S}{\rho C_p}T \tag{3}$$

Here, μ is the dynamic viscosity, ρ is the fluid density, k is the thermal conductivity coefficient and S is a heat source that is defined as follows [14].
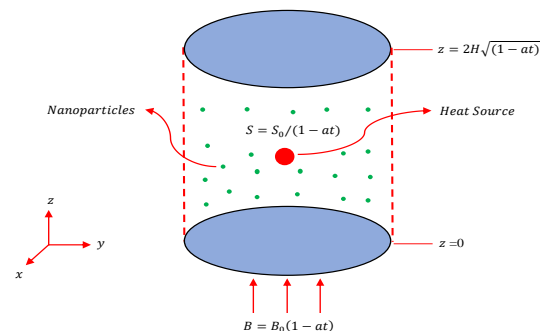

Figure 1. Schematic diagrams of MHD nanofluid flow that compressed between two limited parallel disks

$$S = S_0 / (1 - at) \qquad (4)$$

A magnetic field $\vec{B}$ applied perpendicular to the disk plates goes downwards. Of course, the magnetic Reynolds number is very small and the induced magnetic field is also neglected. So, a magnetic field is defined as follows:

$$\vec{B} = B\vec{e}_y, \quad B = B_0(1 - at) \qquad (5)$$

The electric current $\vec{J}$ and the magnetic field $\vec{B}$ created the electromagnetic force $\vec{F}$ defined as follows:

$$\vec{J} = \sigma[\vec{V} \times \vec{B}]$$
$$\vec{F} = \vec{J} \times \vec{B} = \sigma[\vec{V} \times \vec{B}] \times \vec{B} \qquad (6)$$

We replaced expressions (4), (5), and (6) in momentum and energy equations for the 2D unsteady flow of a nanofluid. So, the following results are obtained [15]:

$$\frac{\partial u}{\partial x} + \frac{\partial v}{\partial y} = 0 \qquad (7)$$

$$\rho_{nf}\left(\frac{\partial u}{\partial t} + u\frac{\partial u}{\partial x} + v\frac{\partial u}{\partial y}\right) = -\frac{\partial p}{\partial x} + \mu_{nf}\left[\frac{\partial^2 u}{\partial x^2} + \frac{\partial^2 u}{\partial y^2}\right] - \sigma_{nf}B^2 u \qquad (8)$$

$$\rho_{nf}\left(\frac{\partial v}{\partial t} + u\frac{\partial v}{\partial x} + v\frac{\partial v}{\partial y}\right) = -\frac{\partial p}{\partial y} + \mu_{nf}\left[\frac{\partial^2 v}{\partial x^2} + \frac{\partial^2 v}{\partial y^2}\right] \qquad (9)$$

$$\frac{\partial T}{\partial t} + u\frac{\partial T}{\partial x} + v\frac{\partial T}{\partial y} = \frac{k_{nf}}{(\rho c_p)_{nf}}\left[\frac{\partial^2 T}{\partial x^2} + \frac{\partial^2 T}{\partial y^2}\right] + \frac{S}{(\rho c_p)_{nf}}T \qquad (10)$$

The boundary conditions for governing equations according to present physics are expressed as follows:

$$v = v_w = dh/dt = -aH/\sqrt{(1 - at)}$$

$$at \quad y = h(t)$$

$$\frac{\partial u}{\partial y} = 0 \quad at \quad y = 0 \qquad (11)$$

$$\frac{\partial T}{\partial y} = 0 \quad at \quad y = 0$$

Some of the governed equations should be changed for modeling the nanofluid because of changes in the fluid thermal conductivity, density, heat capacitance, and electrical conductivity, some of the governed equations

should be changed. Thermo-physical nanofluid properties except for density, which is obtained by Boussinesq approximation, are assumed invariant and are given in Table 1 [16].

The electrical conductivity is written as [17]:

$$\frac{\sigma_{nf}}{\sigma_f} = 1 + \frac{3\left(\frac{\sigma_s}{\sigma_f} - 1\right)\phi}{\left(\frac{\sigma_s}{\sigma_f} + 2\right) - \left(\frac{\sigma_s}{\sigma_f} - 1\right)\phi} \qquad (12)$$

The effect of density at the reference temperature is given by:

$$\rho_{nf} = (1 - \phi)\rho_f + \phi\rho_s \qquad (13)$$

and the heat capacitance of nanofluid can be given as follows [18]:

$$(\rho c_p)_{nf} = (1 - \phi)(\rho c_p)_f + \phi(\rho c_p)_s \qquad (14)$$

The effective thermal conductivity of the component static entities and a Brownian motion part due to micromixing in suspensions were introduced by Koo and Kleinstreuer [19] as follows:

$$k_{eff} = k_{static} + k_{Brownian} \qquad (15)$$

The component static based on Maxwell's classical correlation significantly impacts the effective thermal conductivity.

$$k_{static} = \left(1 + \frac{3\left(\frac{k_s}{k_f} - 1\right)\phi}{\left(\frac{k_s}{k_f} + 2\right) - \left(\frac{k_s}{k_f} - 1\right)\phi}\right)k_f \qquad (16)$$

Koo [20] obtained a particle's Brownian motion via simulating Stokes' flow around a nano-particle and combined the interaction between nano-particles and the temperature effect. So, the Brownian motion part is presented as follows:

$$k_{Brownian} = 5 \times 10^4 \phi \rho_f c_{p,f} \sqrt{\frac{k_s T}{\rho_s d_s}} g'(T, \phi, d_s) \qquad (17)$$

Li [21] developed the g′ function with particle diameter, temperature, and volume fraction.

$$g'(T, \phi, d_s) = (-26.5933 - 0.4038\ln(d_s) - 33.3517\ln(\phi) - 1.9158\ln(\phi)\ln(d_s) + 0.0642\ln(d_s)^2)\ln(T) + (48.4034 - 9.7878\ln(d_s) + 190.2456\ln(\phi) + 10.9285\ln(\phi)\ln(d_s) - 0.7201\ln(d_s)^2) \qquad (18)$$

TABLE 1. Thermo-physical properties of water and nanoparticles [16]

Material	ρ (kg/m^3)	C_P (J/KgK)	K (W/mK)	$\mu \times 10^6$ (Nsm^{-2})	σ (Sm^{-1})
Pure water	997.10	4179	0.613	855	0.05
Copper oxide (Cuo)	6500	540	18	-	5.96×10^7
Alumina (Al2O3)	3970	765	25	-	3.69×10^7

The effective viscosity of the static and a Brownian motion part due to micromixing in suspensions was introduced by Koo and Kleinstreuer [16] as follows:

$$\mu_{eff} = \mu_{static} + \mu_{Brownian} = \mu_{static} + \frac{k_{Brownian}}{k_f} \times \frac{\mu_f}{Pr_f} \tag{19}$$

The viscosity of the nanofluid containing a dilute suspension of small rigid spherical particles is given by the Brinkman model [18] as:

$$\mu_{static} = \frac{\mu_f}{(1-\phi)^{2.5}} \tag{20}$$

For the partial differential Equations 7-10, we introduce the following similarity parameters [22]:

$$\eta = \frac{y}{H\sqrt{1-at}}$$
$$u = \frac{ax}{2(1-at)} f'(\eta)$$
$$v = -\frac{aH}{2\sqrt{1-at}} f(\eta) \tag{21}$$
$$\theta = \frac{T}{T_H}$$

By replacing these parameters in the main equations, the dimensionless equations are as follows:

$$\left(\frac{\mu_{eff}}{\mu_f}\right) f^{(4)} - Sq\left(\frac{\rho_{nf}}{\rho_f}\right)$$
$$[\eta f^{(3)} + 3f'' + f'f'' - ff^{(3)}] - Ha^2\left(\frac{\sigma_{nf}}{\sigma_f}\right) f'' = 0 \tag{22}$$

$$\left(\frac{k_{eff}}{k_f}\right) \theta'' - PrSq\left(\frac{(\rho c_p)_{nf}}{(\rho c_p)_f}\right) [f - \eta] \theta' + S\theta = 0 \tag{23}$$

The boundary conditions for the non-dimensional momentum and energy equations are presented as follows:

$$f(0) = 0, \ f''(0) = 0, \ f(1) = 1,$$
$$f'(1) = 0, \tag{24}$$

$$\theta(1) = 1, \quad \theta'(0) = 0 \tag{25}$$

Here, Ha is the Hartmann number, Sq is the squeeze number, Pr is the Prandtl number and S is the heat source parameter. So, the parameters presented are as follows:

$$Ha = HB_0 \sqrt{\frac{\sigma_f}{\mu_f}} \tag{26}$$

$$Sq = \frac{aH^2}{2v_f} \tag{27}$$

$$Pr = \frac{\mu_f(\rho c_p)_f}{\rho_f k_f} \tag{28}$$

$$S = \frac{S_0 H^2}{k_f} \tag{29}$$

3. SIMULATION METHODOLOGY

3. 1. Radial Basis Function Approximation   The approximate method of the Radial Basis Functions (RBF) is an efficient tool for analyzing functions and equations at high degrees, especially when it is necessary to apply the interpolation problem for scattered data on an irregular geometry [23]. The general form of the radial base function is presented as follows:

$$\Phi[(r)_j] = \Phi(\|x - x_j\|), \ \Phi : \mathcal{R}^d \to \mathcal{R} \tag{30}$$

Here, $r_j = \|x - x_j\|$ is a Euclidean norm, and $x_j, x \in \mathcal{R}^d$. Also, x_j is the center of radial base functions. The interpolation of the radial basis functions is presented as follows:

$$u(x) = \sum_{j=1}^{N} \lambda_j \Phi(\|x - x_j\|) \tag{31}$$

If exist N distinct points $\{x_j\}_{j=1}^{N}$ and values $\{f_j\}_{j=1}^{N}$ such as these points are given, so, coefficients λ_j are specified using the interpolation condition as follows:

$$u(x_j) = f_j, \quad j = 0,1 \dots, N \tag{32}$$

Approximation of function $u(x)$ can be written as a linear combination of the N radial basis function as follows:

$$u(x) = \sum_{j=1}^{N} \lambda_j \Phi_j(x) + \Psi(x) \tag{33}$$

Also, the above approximation can be written without adding Ψ polynomials. In the present study, the radial basis function based on Hardy multiquadric (MQ) is presented as follows:

$$\Phi_j(x) = \sqrt{r_j^2 + \epsilon^2} \tag{34}$$

Here, ϵ, is a shape parameter that significantly affects on the accuracy of the answer [24, 25].

3. 2. Application of RBF   For the application of RBF based on Hardy multiquadric (MQ) on governing equations of the present problem, the general form of the nondimensional momentum and energy equations are considered as follows:

$$f^{(4)} = F(\eta, f, f', f'', f^{(3)})$$
$$\theta'' = \Theta(\eta, \theta, \theta', f) \tag{35}$$

The boundary conditions for governing equations of the present problem are presented as follows:

$$f(0) = 0, \ f''(0) = 0, \ f(1) = 1,$$
$$f'(1) = 0, \ \theta(1) = 1, \quad \theta'(0) = 0. \tag{36}$$

Radial basis function based on Hardy multiquadric (MQ) for nondimensional momentum and energy equations are presented as follows:

$$f(\eta) = \sum_{i=0}^{N} w_i \varphi_i(\eta)$$

$$\theta(\eta) = \sum_{i=0}^{M} v_i \varphi_i(\eta) \tag{37}$$

Also, the *pth* derivation of the nondimensional f function is represented as follows:

$$\frac{d^P f(\eta)}{d\eta^P} = \frac{d^P}{d\eta^P}\left(\sum_{i=0}^{N} w_i \varphi_i(\eta)\right)$$

$$= \sum_{i=0}^{N} w_i (d^P \varphi_i(\eta)/d\eta^P)$$

$$= \sum_{i=0}^{N} w_i h_i^{[p]}(\eta) \tag{38}$$

Nondimensional θ is represented according to Equation (38), so, with applied the Equations (37) and (38) into Equation (35):

$$\sum_{i=0}^{N} w_i h_i^{[4]}(\eta) =$$
$$F\begin{pmatrix} \eta, \sum_{i=0}^{N} w_i \varphi_i(\eta), \sum_{i=0}^{N} w_i h_i^{[1]}(\eta), \\ \sum_{i=0}^{N} w_i h_i^{[2]}(\eta), \sum_{i=0}^{N} w_i h_i^{[3]}(\eta) \end{pmatrix}$$

$$\sum_{i=0}^{M} v_i h_i^{[2]}(\eta) =$$
$$\Theta\begin{pmatrix} \eta, \sum_{i=0}^{M} v_i \varphi_i(\eta), \sum_{i=0}^{M} v_i h_i^{[1]}(\eta), \\ \sum_{i=0}^{N} w_i \varphi_i(\eta) \end{pmatrix} \tag{39}$$

Set the residual (39) equal to zero at the set of collocation points η_j as follows:

$$\sum_{i=0}^{N} w_i h_i^{[4]}(\eta_j) -$$
$$F\begin{pmatrix} \eta_j, \sum_{i=0}^{N} w_i \varphi_i(\eta_j), \sum_{i=0}^{N} w_i h_i^{[1]}(\eta_j), \\ \sum_{i=0}^{N} w_i h_i^{[2]}(\eta_j), \sum_{i=0}^{N} w_i h_i^{[3]}(\eta_j) \end{pmatrix} = 0$$

$$\sum_{i=0}^{M} v_i h_i^{[2]}(\eta_j) -$$
$$\Theta\begin{pmatrix} \eta_j, \sum_{i=0}^{M} v_i \varphi_i(\eta_j), \sum_{i=0}^{M} v_i h_i^{[1]}(\eta_j), \\ \sum_{i=0}^{N} w_i \varphi_i(\eta_j) \end{pmatrix} = 0 \tag{40}$$

Then, for solving *M+N-4* nonlinear equations, we set the boundary conditions (36) as follows:

$$f(0) = \sum_{i=0}^{N} w_i \varphi_i(0) = 0,$$

$$f''(0) = \sum_{i=0}^{N} w_i h_i^{[2]}(0) = 0,$$

$$f(1) = \sum_{i=0}^{N} w_i \varphi_i(1) = 1,$$

$$f'(1) = \sum_{i=0}^{N} w_i h_i^{[1]}(1) = 0,$$

$$\theta(1) = \sum_{i=0}^{M} v_i \varphi_i(1) = 1,$$

$$\theta'(0) = \sum_{i=0}^{M} w_i h_i^{[1]}(0) = 0. \tag{41}$$

Equations (40) and (41) are represented the *M+N+2* nonlinear equations and unknowns, and with solving these equations, w_i and v_i are obtained. So, by substituting w_i and v_i at Equations (37), f and θ are obtained.

3. 3. Application of Akbari-Ganji's Method
This method has been presented by Akbari-Ganji and applied by many researchers [26-30]. For the application of AGM to the nondimensional momentum and energy

equations, the detail of these equations are considered as follows:

$$F(\eta) = \left(\frac{\mu_{eff}}{\mu_f}\right)f^{(4)} - Sq\left(\frac{\rho_{nf}}{\rho_f}\right)[\eta f^{(3)} + 3f'' +$$
$$f'f'' - ff^{(3)}] - Ha^2\left(\frac{\sigma_{nf}}{\sigma_f}\right)f'' = 0$$

$$\Theta(\eta) = \left(\frac{k_{eff}}{k_f}\right)\theta'' - PrSq\left(\frac{(\rho c_p)_{nf}}{(\rho c_p)_f}\right)[f - \eta]\theta' +$$
$$S\theta = 0 \tag{42}$$

Total answers with constant coefficients for nondimensional momentum and energy equations are considered as follows:

$$f(\eta) = a_0.\eta^0 + a_1.\eta^1 + a_2.\eta^2 + a_3.\eta^3$$
$$+a_4.\eta^4 + a_5.\eta^5, \tag{43}$$
$$\theta = b_0.\eta^0 + b_1.\eta^1 + b_2.\eta^2 + b_3.\eta^3.$$

Equation (43) sustituted into governing Equations (42) and considered boundary conditions as follows:

$$f(0) = 0, \frac{d^2 f}{d\eta^2}(0) = 0,$$

$$f(1) = 1, \frac{df}{d\eta}(1) = 0, \tag{44}$$

$$\theta(1) = 1, \frac{d\theta}{d\eta}(0) = 0$$

Since the proposed problem engaged with four trial functions which contain ten constant coefficients and this geometry has six equations according to Equation (44) and created four additional equations in the following order:
$F(0) = 0, F(1) = 0, \Theta(0) = 0, \Theta(1) = 0.$
So by utilizing the above procedures, we have obtained a set of polynomials containing ten equations and ten constants which by solving them we would be able to obtain Equation (43). By substituting obtained constant coefficients from mentioned procedures, Equation (43) could easily be yielded nondimensional momentum and energy equations, respectively as follows:

$$f(\eta) = -0.4816\eta^5 + 0.4631\eta^3 + 1.0184\eta$$
$$\theta(\eta) = 0.1902\eta^3 + 0.2699\eta^2 + 0.5399 \tag{45}$$

3. 4. Differential Transform Method (DTM)
Basic definitions and operations of differential transformation are introduced as follows. Differential transformation of the function $f(\eta)$ is defined as follows:

$$F(k) = \frac{1}{k!}\frac{d^k f(\eta)}{d\eta^k}\Big|_{\eta=\eta_0} \tag{46}$$

In Equation (46), $f(\eta)$ is the original function and $F(k)$ is the transformed function which is called the T-function (it is also called the spectrum of the $f(\eta)$ at $\eta = \eta_0$, in the k domain). The differential inverse transformation of $F(k)$ is defined as:

$$f(\eta) = \sum_{k=0}^{\infty} F(k)(\eta - \eta_0)^k \tag{47}$$

By combining Equations (46) and (47) $f(\eta)$ can be obtained:

$$f(\eta) = \sum_{k=0}^{\infty} \left[\frac{d^k f(\eta)}{d\eta^k} \Big|_{\eta=\eta_0} \right] \frac{(\eta-\eta_0)^k}{k!} \qquad (48)$$

Equation (48) implies that the concept of the differential transformation is derived from Taylor's series expansion, but the method does not evaluate the derivatives symbolically. However, relative derivatives are calculated by an iterative procedure that is described by the transformed equations of the original functions. From the definitions of Eqautions (46) and (47), it is easily proven that the transformed functions comply with the basic mathematical operations shown below. In real applications, the function $f(\eta)$ in Equation (48) is expressed by a finite series and can be written as:

$$f(\eta) = \sum_{k=0}^{N} F(k)(\eta - \eta_0)^k \qquad (49)$$

Equation (49) implies that $f(\eta) = \sum_{k=N+1}^{\infty} F(k)(\eta - \eta_0)^k$ is negligibly small, where N is series size. Theorems to be used in the transformation procedure, which can be evaluated from Equations (46) and (47), are given by Sheikholeslami and Domairry Ganji [31]. Also, refer to the same reference to solve the model with DTM.

3. 5. Validation for Analytical Methods   The comparison and verification between the simulation of the nondimensional velocity profile of CuO-water multiphase fluid flow and the Differential Transformation Method (DTM) by Sheikholslami and Domiri Ganji. [31] is represented in Figure 2. This figure shows the velocity profiles are close together and according to the physical condition of the problem, there is good accuracy between the Akbari-Ganji's Method (AGM) and Radial Basis Function approximation (RBF) based on Hardy multiquadric (MQ) function and DTM [31].
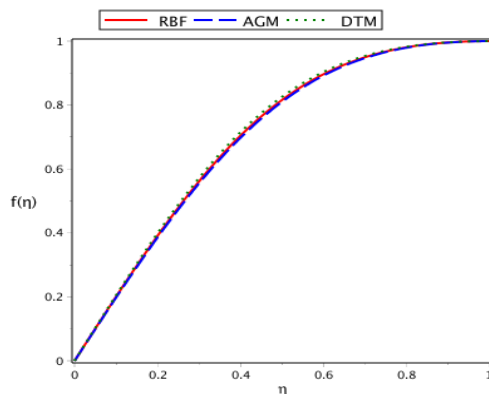

Figure 2. Comparison of the nondimensional velocity profile of CuO-water multiphase fluid flow (present work) and DTM for previous work ([31]) at $S = -1$, $Pr = 6.2$, $Ha = 8$, and $Sq = 1$.

Table 2, represented the numerical comparison between the Akbari-Ganji's Method (AGM), Radial Basis Function approximation (RBF) based on Hardy multiquadric (MQ) function, and Differential Transformation Method (DTM) as shown in Figure 2.

4. RESULTS AND DISCUSSION

In this research, Brownian motion with heat source effects between parallel disks on nondimensional velocity and temperature fields are illustrated. Also, electromagnetic force effects on squeezing flow between parallel disks are surveyed. Figure 3 is represented the effect of squeeze number on nondimensional velocity and temperature profiles of copper oxide (CuO) nanoparticles. The velocity and temperature profiles are depicted using Akbari-Ganji's Method (AGM) and Radial Basis Function approximation (RBF) based on Hardy multiquadric (MQ) function. At the AGM method, the vertical velocity of nanofluid flow is increased with increasing squeeze number, and with extending more than $Sq = 1$, the concavity of the diagrams is close to each other and almost coincides. But at a squeeze number more than $Sq = 1$, the vertical velocity profile of nanofluid flow is slightly reduced. At the RBF method, the vertical velocity of the nanofluid is increased with the enhancement of the squeeze number. The graphs converge and the vertical velocity of the nanoparticles is not changed significantly because the graphs are matched together.

The numerical values of nondimensional velocity and temperature of CuO nanoparticles are illustrated at AGM and RBF (MQ) methods and the numerical difference ($|\Delta| = |AGM - RBF|$) between them in Tables 3-5.

TABLE 2. Numerical comparison between AGM, RBF, and DTM for nondimensional velocity profile of CuO-water multiphase fluid flow at $S = -1$, $Pr = 6.2$, $Ha = 8$, and $Sq = 1$

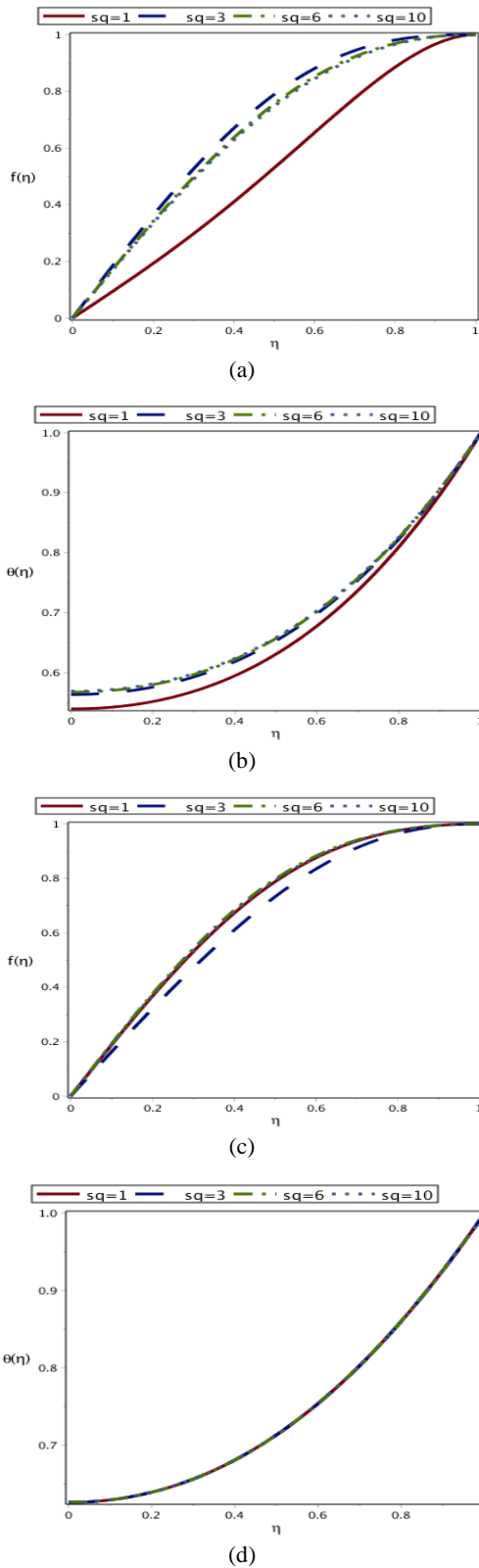| η	RBF	AGM	DTM [31]
0.0	0	0	0
0.1	0.1984	0.1964	0.2033
0.2	0.3871	0.3834	0.3962
0.3	0.5566	0.5518	0.5683
0.4	0.6994	0.6943	0.7116
0.5	0.8116	0.8072	0.8225
0.6	0.8933	0.8900	0.9014
0.7	0.9477	0.9457	0.9526
0.8	0.9800	0.9791	0.9821
0.9	0.9957	0.9955	0.9962
1.0	1	1	1

(a)

(b)

(c)

(d)

Figure 3. Comparison between AGM (a,b) and RBF (c,d) for effects of squeeze number on dimensionless vertical velocity and temperature profile for CuO-water multiphase fluid flow at $S = -1$, $Pr = 6.2$ and $Ha = 1$

TABLE 3. Numerical comparison of vertical velocity between AGM and RBF for CuO-water multiphase fluid flow at $Ha = 1$, $S = -1$, $Pr = 6.2$, $Sq = 3$.

η	f		
	AGM	**RBF(MQ)**	**|Δ|**
0.0	0	0	0
0.1	0.1850	0.1629	0.0221
0.2	0.3628	0.3215	0.0413
0.3	0.5265	0.4718	0.0547
0.4	0.6702	0.6104	0.0598
0.5	0.7894	0.7330	0.0564
0.6	0.8810	0.8350	0.0460
0.7	0.9445	0.9126	0.0319
0.8	0.9816	0.9643	0.0173
0.9	0.9973	0.9920	0.0053
1.0	1	1	1

TABLE 4. Numerical comparison of horizontal velocity between AGM and RBF for CuO-water multiphase fluid flow at $Ha = 1$, $S = -1$, $Pr = 6.2$, $Sq = 3$.

| η	f'		
	AGM	**RBF(MQ)**	**|Δ|**
0.0	1.8623	1.6372	0.2251
0.1	1.8257	1.6142	0.2115
0.2	1.7182	1.5501	0.1681
0.3	1.5463	1.4507	0.0956
0.4	1.3209	1.3135	0.0074
0.5	1.0571	1.1310	0.0739
0.6	0.7745	0.9031	0.1286
0.7	0.4971	0.6463	0.1492
0.8	0.2531	0.3913	0.1382
0.9	0.0751	0.1695	0.0944
1.0	0	0	0

These Tables are shown at $Sq = 3$ and $\eta = 0$, the maximum difference in horizontal velocity is 0.2251 and the minimum difference at $\eta = 0.9$ is 0.0053. Also, the nondimensional temperature at $\eta = 0.3$ and $\eta = 0.4$ has a maximum difference of 0.0627 and the minimum difference at $\eta = 0.9$ is equal to 0.0213.

Figure 4 represents the effects of squeeze number on nondimensional vertical velocity and temperature profile for Al₂O₃-water multiphase fluid flow using AGM and RBF (MQ) at $S = -1$, $Pr = 6.2$, and $Ha = 1$.

This figure has depicted the same behavior as CuO-water multiphase fluid flow; however, there is no

TABLE 5. Numerical comparison of temperature between AGM and RBF for CuO-water multiphase fluid flow at $Ha = 1, S = -1, Pr = 6.2, Sq = 3$.
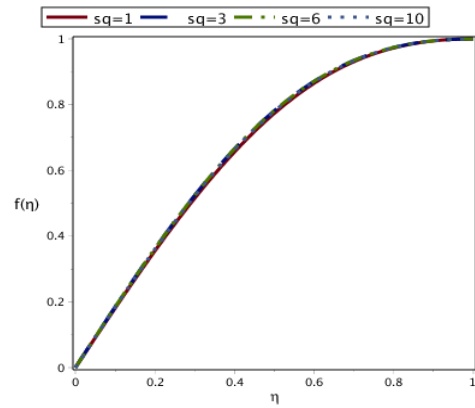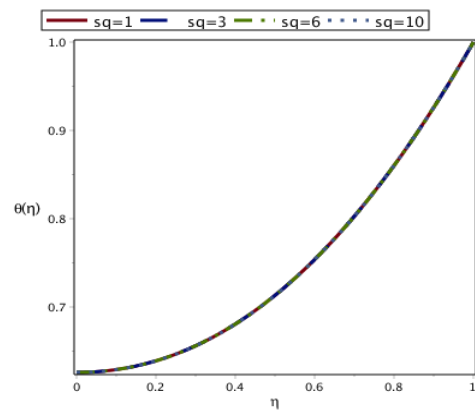
|	θ		
η	AGM	RBF (MQ)	$|\Delta|$
0.0	0	0	0
0.1	0.1850	0.1629	0.0221
0.2	0.3628	0.3215	0.0413
0.3	0.5265	0.4718	0.0547
0.4	0.6702	0.6104	0.0598
0.5	0.7894	0.7330	0.0564
0.6	0.8810	0.8350	0.0460
0.7	0.9445	0.9126	0.0319
0.8	0.9816	0.9643	0.0173
0.9	0.9973	0.9920	0.0053
1.0	1	1	1
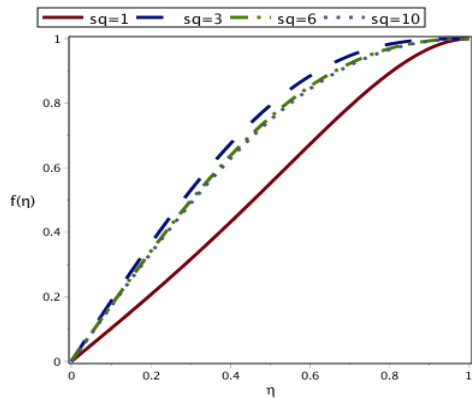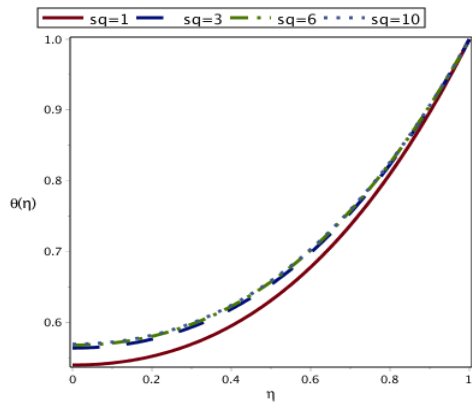
(c)

(d)

Figure 4. Comparison between AGM(a,b) and RBF (c,d) for effects of squeeze number on dimensionless vertical velocity and temperature profile for Al2O3-water multiphase fluid flow at S=−1, Pr=6.2, and Ha=1.


(a)

(b)

significant change with increasing the squeeze number on this nanofluid in the RBF method.

Figure 5 investigated the effect of the Hartmann number on Alumina (Al$_2$O$_3$)-water multiphase fluid flow using AGM and RBF methods. With an increase in the Hartmann number, the nanofluid's nondimensional horizontal and vertical velocities are increased using the AGM method. Except for $Ha = 0$, the graphs converged together and the heat transfer didn't change by increasing the Hartmann number. With increasing Hartmann number, the nondimensional horizontal and vertical velocities of nanofluid are increased, the graphs converged together, and the heat transfer didn't change using the RBF method.
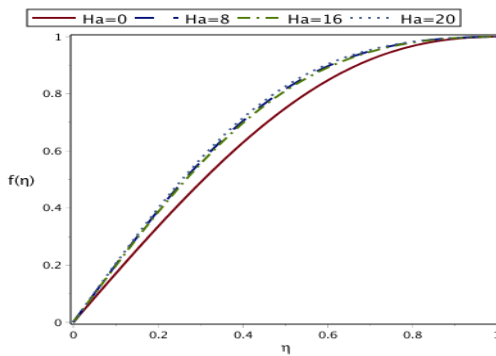
Figure 6 illustrated the effect of the Prandtl number on the nondimensional temperature profiles of Al$_2$O$_3$ and CuO nanofluids using the AGM method. According to this figures., maximum values for nondimensional temperature profile were at $Pr = 2$.
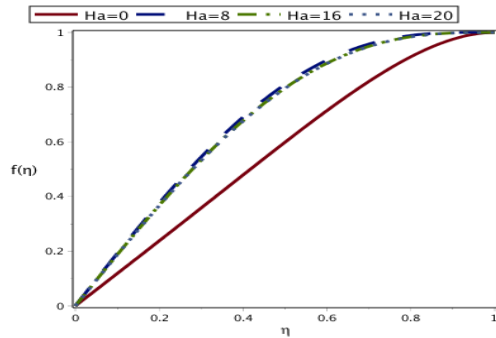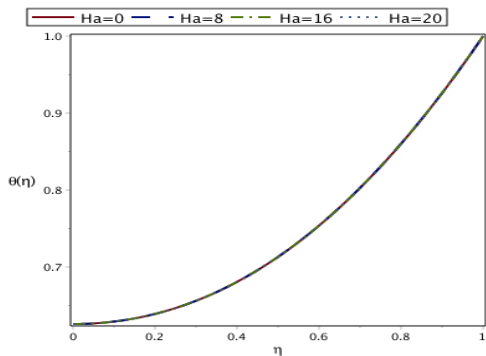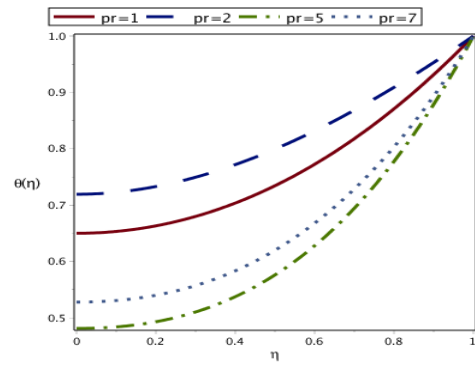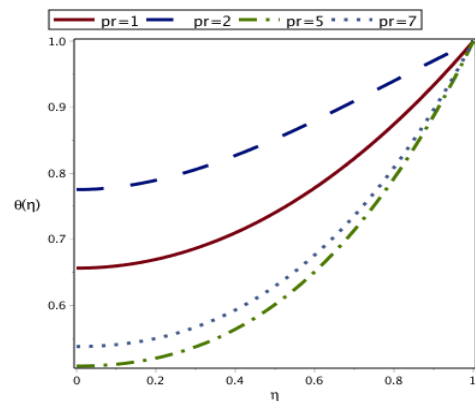
(a)
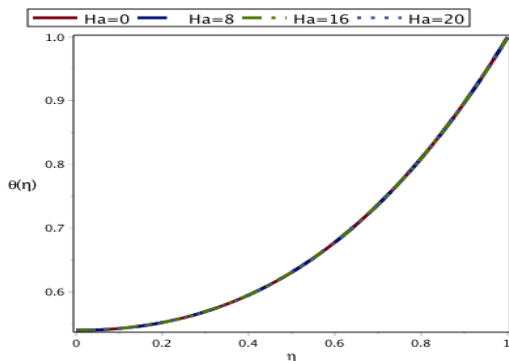
(b)

(c)

(d)

Figure 5. Comparison between AGM (a,b) and RBF (c,d) for effects of Hartman number on dimensionless vertical velocity and temperature profile for Al2O3-water multiphase fluid flow at $S=-1$, $Pr=6.2$, and $Sq=1$

Alumina (Al$_2$O$_3$)

Copper oxide (CuO)

Figure 6. Comparison between Al2O3 and CuO nanoparticles for effects of Prandtl number on dimensionless temperature profile at $S=-1$, $Sq=1$, and $Ha=1$.

Figure 7 shows the residual error function graph for the Al$_2$O$_3$ nanoparticle because there is no exact solution in this geometry, we obtain the residual error function using the RBF method.
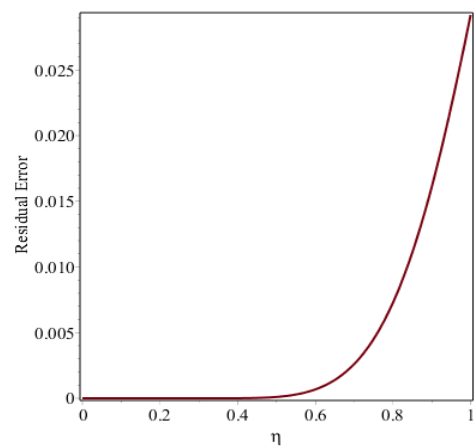

Figure 7. Graph of residual error function using RBF method on velocity profile for Al$_2$O$_3$-water multiphase fluid flow at $S = -1$, $Pr = 6.2$, and $Sq = 1$.

5. CONCLUSION

In the present study, squeezing flow with Brownian motion effects on nondimensional vertical, horizontal velocity, and temperature profiles were surveyed between parallel disks with a heat source. Also, for simulating the nanoparticle effects on nondimensional temperature fields and velocity profiles were used the Akbari-Ganji's Method (AGM) and Radial Basis Function approximation (RBF) were based on Hardy multiquadric (MQ) function. We investigated Al_2O_3 and CuO nanoparticle's effects on nondimensional velocity and temperature fields between parallel disks with a heat source and electromagnetic force. Finally, some of the main points are summarized:

- The effects of squeezes number on nondimensional horizontal and vertical velocity and temperature field for Al_2O_3 and CuO nanoparticles have a similar behaviour using the AGM method.

- With increasing the squeezes number on Al_2O_3 and CuO nanofluid flow, the nondimensional temperature field did not change using the RBF method.

- The minimum difference between AGM and RBF methods for nondimensional vertical velocities field at $\eta = 0.9$ and $Ha = 8$.

- The effects of the Hartmann number on nondimensional vertical velocities field for Al_2O_3 nanoparticles at $\eta = 0$ have a slight difference from the other Hartmann values using the AGM method.

- Also, increasing the Prandtl number for Al_2O_3 and CuO nanoparticles in AGM and RBF methods, decreased the nondimensional temperature field, which has the minimum difference between AGM and RBF methods at $Pr = 1$, $\eta = 0.9$ is equal to 0.0019.

6. REFERENCES

1. Hosseinzadeh, Kh., Alizadeh, M., and Ganji, D. D., "Hydrothermal Analysis on MHD Squeezing Nanofluid Flow in Parallel Plates by Analytical Method," *International Journal of Mechanical and Materials Engineering*, Vol. 15, No. 8 (2020). https://doi.org/ 10.1186/s40712-018-0089-7

2. Asefi, M., Molavi, H., Shariaty-Niassar, M., babaee Darband, j., Nemati, N., Yavari, M., and Akbari, M., "An Investigation on Stability, Electrical and Thermal Characteristics of Transformer Insulating Oil Nanofluids," *International Journal of Engineering, Transactions A: Basics,* Vol. 29, No. 10, (2016), 1332-1340. https://doi.org/0.5829/idosi.ije.2016.29.10a.02

3. Ravindran, R., Ganapathirao, M., Pop, I., "Effects of Chemical Reaction and Heat Generation/Absorption on Unsteady Mixed Convection MHD Flow Over A Vertical Cone With Non-Uniform Slot Mass Transfer," *International Journal of Heat and Mass Transfer*, Vol. 73, (2014), 743-751. https://doi.org/ 10.1016/j.ijheatmasstransfer.2014.02.053

4. Motahar, S., "A Neural Network Approach to Estimate Non-Newtonian Behavior of Nanofluid Phase Change Material Containing Mesoporous Silica Particles, " *International Journal of Engineering, Transactions B: Applications,* Vol. 34, No. 08, (2021), 1974-1981. https://doi.org/10.5829/ije.2021.34.08b.18

5. Asgari, M., Tariverdilo, S., "Investigating The Seismic Response of Structural Walls Using Nonlinear Static and Incremental Dynamic Analyses, " *International Journal of Engineering, Transactions B: Applications,* Vol. 30, No. 11, (2017), 1691-1699. https://doi.org/10.5829/ije.2017.30.11b.09

6. Han He, Ji., Mostapha, Doaa R., "Insight into the Significance of Hall Current and Joule Heating on the Dynamics of Darcy–Forchheimer Peristaltic Flow of Rabinowitsch Fluid, " *Journal of Mathematics*, (2021) Article ID 3638807. https://doi.org/10.1155/2021/3638807

7. Han He, Ji., Abed Elzam., N. Y., "Insights into partial slips and temperature Jumps of a nanofluid flow over a stretched or shrinking surface, "*Journal of Energies*, Vol. 14, No. 20, (2021), 6691. https://doi.org/10.3390/en14206691

8. Rashidi, M. M., Alhuyi Nazari, M., Mhariq, I, Ali, N,"Modeling and Sensitivity Analysis of thermal Conductivity of Ethylene Glycol-Water Based Nanofluids with Alumina Nanoparticles, " *Computations & Experiments on Dynamics of Complex Fluid & Structure*, (2022) 1-8. https://doi.org/10.1007/s40799-022-00567-4

9. Alagumalai, A., Qin, C., Vimal, K.E.K., Solomin, E., Yang, L., Zhang, P., Otanicar, T., Kasaeian, A., Chamkha, A.J., Rashidi, M.M. and Wongwises, S., "Conceptual Analysis Framework Development to Understand Barriers of Nanofluid Commercialization, "*Journal of Nano Energy*, Vol. 92, (2022), 106736. https://doi.org/ 10.1016/j.nanoen.2021.106736

10. Nouri, K., Nazari, M., and Torkzadeh, L., "Numerical Approximation of The System of Fractional Differential Equations with Delay and Its Applications," *The European Physical Journal Plus*, Vol. 135, No. 3, (2020) 1-14. https://doi.org/10.1140/epjp/s13360-020-00351-6

11. Nouri, K., Baleanu, D., and Torkzadeh, L., "Study on Application of Hybrid Functions To Fractional Differential Equations," *Iranian Journal of Science and Technology,* Transactions A: Science, Vol. 42, No. 4, (2018), 1343-1350. https://doi.org/ 10.1007/s40995-017-0224-y

12. Dadsetadi, S., Nouri, K., and Torkzadeh, L., "Solvability of Some Nonlinear Integro-Differential Equations of Fractional Order Via Measure of Noncompactnes," *The Pure and Applied Mathematics,* Vol. 27, No. 1, (2020), 13-24. https://doi.org/10.7468/jksmeb.2020.27.1.13

13. Pourziaei Araban. H., Alinejad, J., Peiravi, M. M., and Domairry Ganji, D., "3D Numerical Simulation of Cavity with Bottom Heat Source for Ra-Nu Correlation," *Transport Phenomena Nano Micro Scales*, (2021). https://doi.org/10.1140/epjp/s13360-020-00351-6

14. Eringen, A., "Theory of Micropolar Fluids," *Journal of Mathmatics*, Vol. 16, No. 1, (1966), 1-18.

15. Mustafa, M., Hayat, T., and Obaidat, S., "On Heat And Mass Transfer in The Unsteady Squeezing Flow Between Parallel Plates," *Meccanica*, Vol. 47, No. 7, (2012), 1581-1589. https://doi.org/ 10.1007/s11012-012-9536-3

16. Koo, J., and Kleinstreuer, C., "Laminar Nanofluid Flow in Micro heat-Sinks," *International Journal of Heat and Mass Transfer*, Vol. 48, No. 7, (2005), 2652-2661. https://doi.org/ 10.1016/j.ijheatmasstransfer.2005.01.029

17. Salehi, S., Nori, A., Hosseinzadeh, Kh., and Ganji, D. D., "Hydrothermal Analysis Of MHD Squeezing Mixture Fluid Suspended By Hybrid Nanoparticles Between Two Parallel Plates," *Case Studies in Thermal Engineering*, Vol. 21, (2020) 100650. https://doi.org/ 10.1016/j.csite.2020.100650

18. Zhang, B., Song, Z., and Mao, W., "A Novel Wake Energy Reuse Method to Optimize The Layout For Savonius-Type Vertical Axis Wind Turbines," *Energy*, Vol. 121, No. 7, (2017), 341-355. https://doi.org/ 10.1016/j.energy.2017.01.004

19. Koo, J., and Kleinstreuer, C., "Viscous Dissipation Effects In Micro Tubes And Micro Channels," *International Journal of Heat and Mass Transfer,* Vol. 47, No. 7, (2004), 3159–3169. https://doi.org/ 10.1016/j.ijheatmasstransfer.2004.02.017

20. Koo, J., "Computational Nanofluid Flow and Heat Transfer Analyses Applied to Microsystems," (Ph.D. thesis), NC State University, Raleigh, NC, (2004).

21. Li, J., "Computational Analysis of Nanofluid Flow in Micro Channels With Applications to Micro-Heat Sinks And Bio-MEMS," (Ph.D. thesis), NC State University, Raleigh, NC, (2008).

22. Singh, K., Rawat, S. K., and Kumar, M., "Heat and Mass Transfer on Squeezing Unsteady MHD Nanofluid Flow between Parallel Plates with Slip Velocity Effect," *Journal of Nanoscience*, (2016). https://doi.org/ 0.1155/2016/9708562

23. Cheng, A. H. D., Golberg, M. A., Kansa, E. J., and Zammito, G., "Exponential Convergence And H-C Multiquadric Collocation Method For Partial Differential Equations," *Numerical Methods Partial Differential Equations*, Vol. 19, No. 1, (2003), 571-594. https://doi.org/ 10.1002/num.10062

24. Elansari, M., Ouazar, D., and Cheng, A. H. D., "Boundary Solution of Poisson's Equation Using Radial Basis Function Collocated on Gaussian Quadrature Nodes," *Communications in Numerical Methods in Engineering*, Vol. 17, No. 7, (2001), 455-464. https://doi.org/ 10.1002/cnm.419

25. Haq, S., Hussain, A., and Uddin, M., "On The Numerical Solution of Nonlinear Burgers-Type Equations Using Meshless Method Of Lines," *Applied Mathematics and Computation*, Vol. 218, No. 1, (2012), 6280-6290. https://doi.org/ 10.1016/j.amc.2011.11.106

26. Peiravi, M. M., Alinejad, J., Domairry Ganji, D., and Maddah, S., "Numerical Study of Fins Arrangement and Nanofluids Effects on Three-Dimensional Natural Convection in The Cubical Enclosure," *Transport Phenomena Nano Micro Scales*, Vol. 7, No. 2, (2019), 97-112. https://doi.org/ 10.22111/TPNMS.2019.4845

27. Peiravi, M. M., and Alinejad, J., "Hybrid Conduction, Convection, and Radiation Heat Transfer Simulation in A Channel with Rectangular Cylinder," *Journal of Thermal Analysis and Calorimetry*, Vol. 140, No. 6, (2020), 2733-2747. https://doi.org/ 10.1007/s10973-019-09010-0

28. Peiravi, M. M., Alinejad, J., Domairry Ganji, D., and Maddah, S., "3D Optimization of Baffle Arrangement in A Multi-Phase Nanofluid Natural Convection Based on Numerical Simulation," *International Journal of Numerical Methods for Heat and Fluid Flow*, Vol. 30, No. 5, (2019), 2583-2605. https://doi.org/ 10.1108/HFF-01-2019-0012

29. Alinejad, J., Peiravi, M. M., "Numerical analysis of secondary droplets characteristics due to drop impacting on 3D cylinders considering dynamic contact angle," *Meccanica*, Vol. 55, No. 10, (2020), 1975-2002. https://doi.org/ 10.1007/s11012-020-01240-z

30. Domairry Ganji, D., Peiravi, M. M., and Abbasi, M., "Evaluation of The Heat Transfer Rate Increases in Retention Pools Nuclear Waste," *International Journal of Nano Dimension*, Vol. 6, No. 4, (2015), 385-398.

31. Sheikholeslami, M, Domairry Ganji, D., "Nanofluid Flow and Heat Transfer Between Parallel Plates Considering Brownian Motion Using DTM, " *Computer Methods in Applied Mechanics and Engineering,* 283, (2015), 651-663. https://doi.org/10.1140/epjp/s13360-020-00351-6

Persian Abstract

چکیده

نوآوری مقاله حاضر بررسی تحلیلی اثرات حرکت براونی بر جریان نانوسیال و نیروی الکترومغناطیسی بین دیسک‌های موازی با منبع حرارت است. اثرات نانوذرات بر میدان دمایی بی‌بعد و سرعت جریان سیال با استفاده از روش اکبری گنجی و تقریب تابع پایه شعاعی بر اساس تابع چند مربعی هاردی تحلیل شده است. روش اکبری گنجی یک روش تحلیلی قوی است که هر معادله دیفرانسیل خطی و غیرخطی را با هر درجه ای از متغیرها حل می‌کند. توابع پایه شعاعی یک روش تقریبی برای تجزیه و تحلیل توابع و معادلات در درجات بالا است، به ویژه زمانی که لازم است مسئله درون یابی برای داده‌های پراکنده در هندسه نامنظم اعمال شود. نتایج نشان داد که حداکثر تفاوت بین روش‌های اکبری گنجی و تابع پایه شعاعی برای سرعت افقی بی‌بعد روی نانوسیال CuO در Sq = 1 و η = 0 برابر ۰.۲۲۵۱ و حداقل تفاوت برای سرعت عمودی بی‌بعد نانوسیال Al₂O₃ در η = 0 برابر با ۰.۰۰۱۸ است. همچنین اثرات عدد هارتمن بر میدان سرعت‌های افقی و عمودی بی‌بعد برای نانوذرات Al₂O₃ در η = 0 تفاوت جزئی با سایر مقادیر هارتمن با استفاده از روش AGM دارد. حداکثر سرعت های افقی بی‌بعد در η = 0 و Ha = 8 برابر با ۱.۹۳۵٤ است.